INSTITUTE OF PHYSICS PUBLISHING PHYSICS IN MEDICINE AND BIOLOGY

Phys. Med. Biol. **50** (2005) 3007–3022 doi:10.1088/0031-9155/50/13/003

Use of the isolated problem approach for multi-compartment BEM models of electro-magnetic source imaging

Nevzat G Gençer and Zeynep Akalın-Acar

Department of Electrical and Electronics Engineering, Brain Research Laboratory, Middle East Technical University, 06531 Ankara, Turkey

E-mail: ngencer@metu.edu.tr

Received 4 February 2005, in final form 29 April 2005
Published 8 June 2005
Online at stacks.iop.org/PMB/50/3007

Abstract

The isolated problem approach (IPA) is a method used in the boundary element method (BEM) to overcome numerical inaccuracies caused by the high-conductivity difference in the skull and the brain tissues in the head. Hämäläinen and Sarvas (1989 *IEEE Trans. Biomed. Eng.* **36** 165–71) described how the source terms can be updated to overcome these inaccuracies for a three-layer head model. Meijs *et al* (1989 *IEEE Trans. Biomed. Eng.* **36** 1038–49) derived the integral equations for the general case where there are an arbitrary number of layers inside the skull. However, the IPA is used in the literature only for three-layer head models. Studies that use complex boundary element head models that investigate the inhomogeneities in the brain or model the cerebrospinal fluid (CSF) do not make use of the IPA. In this study, the generalized formulation of the IPA for multi-layer models is presented in terms of integral equations. The discretized version of these equations are presented in two different forms. In a previous study (Akalın-Acar and Gençer 2004 *Phys. Med. Biol.* **49** 5011–28), we derived formulations to calculate the electroencephalography and magnetoencephalography transfer matrices assuming a single layer in the skull. In this study, the transfer matrix formulations are updated to incorporate the generalized IPA. The effects of the IPA are investigated on the accuracy of spherical and realistic models when the CSF layer and a tumour tissue are included in the model. It is observed that, in the spherical model, for a radial dipole 1 mm close to the brain surface, the relative difference measure (RDM*) drops from 1.88 to 0.03 when IPA is used. For the realistic model, the inclusion of the CSF layer does not change the field pattern significantly. However, the inclusion of an inhomogeneity changes the field pattern by 25% for a dipole oriented towards the inhomogeneity. The effect of the IPA is also investigated when there is an inhomogeneity in the brain. In addition to a considerable change in the scale of the potentials,

the field pattern also changes by 15%. The computation times are presented for the multi-layer realistic head model.

1. Introduction

Localization of the brain activities using electroencephalography (EEG) and magnetoencephalography (MEG) measurements is called electro-magnetic source imaging (EMSI) (Baillet *et al* 2001, Michel *et al* 2001, He 1998, Gençer *et al* 2003). The *forward problem* of EMSI is the solution of the scalp potentials and magnetic fields due to a given source configuration. To solve the potential distribution due to electrical sources in the brain, various numerical methods can be used. For compartmental models of the head, the boundary element method (BEM) is frequently employed. In the BEM implementations, generally, the three-shell model of the head is used to model the scalp, skull and the brain tissues. However, the low conductivity of the skull layer results in inaccuracy in the solutions of the resultant system of equations. To increase the accuracy, the isolated problem approach (IPA) is employed and a modified set of equations is solved (Meijs *et al* 1989, Hämäläinen and Sarvas 1989). When the white matter, grey matter, a (large) ventricle or a tumour in the brain is to be modelled, i.e., when more realistic head models are to be used, the IPA can still be applied. For that purpose, a general formulation was provided in the literature (Meijs *et al* 1989); however, its numerical implementation has not been attempted by others in this field. In this study, the generalized version of IPA is investigated using spherical and realistic head models. The extended forms of the modified source terms are derived. Two different forms of the discretized version are presented to apply the IPA when the BEM is used for a multi-compartment tissue model in the skull. Numerical solutions for a realistic head model are provided.

Realistic modelling of the human head is necessary to increase the accuracy of EMSI solutions. Roth *et al* (1993), Crouzeix *et al* (1999) and Cuffin (1996) investigated dipole localization accuracy using spherical and realistic meshes. It was shown that a realistic model improves the localization accuracy on the order of 1–2 cm. However, in those studies, the realistic models have only three tissue types, namely, the scalp, skull and the brain. Ramon *et al* (2004) examined the effects of soft skull bone, cerebrospinal fluid (CSF) and grey matter on scalp potentials using the finite element method (FEM). They observed that the scalp potentials were significantly affected by these tissues. Thus, the accuracy in the source localization can further be improved if more realistic head models are used in the forward problem solutions.

To improve the accuracy of the BEM models, several approaches have been used. Higher order elements (Budiman and Buchanan 1993, Gençer and Tanzer 1999, Frijns *et al* 2000), various integration techniques (Fuchs *et al* 1998) and the IPA (Meijs *et al* 1989, Hämäläinen and Sarvas 1989) are among these approaches. In a previous study, an advanced realistic BEM implementation that can model intersecting tissue boundaries was described (Akalın-Acar and Gençer 2004). The model makes use of quadratic elements, recursive integration and the IPA to improve the accuracy of the BEM solutions. However, the transfer matrix formulations were valid for a head model with a single layer inside the skull. They were not in a general form to include the effects of tissue types, such as CSF, white matter, grey matter, a possible ventricle or a tumour in the brain. A general IPA formulation is required when more detailed head models are used.

The IPA is a method to overcome numerical inaccuracies caused by high-conductivity difference between the skull and the inner layers (CSF or brain). Hämäläinen and Sarvas

(1989) formulated the IPA for a three-layer head model when there exists a single isolated layer (i.e., there is only brain inside the skull). In that study, a modified set of equations was derived and the results were compared with the analytical solutions. Meijs *et al* (1989) derived integral equations to use the IPA with multi-layer head models assuming multiple isolated layers. However, to the knowledge of the authors, such use has not been numerically implemented by other researchers. The researchers who use models with more than three layers have not applied the IPA (Frijns *et al* 2000, van Burik and Peters 2000, Babiloni *et al* 2001). Meijs *et al* (1989) tested the accuracy of solutions using a four-shell spherical model with linear elements, and concluded that the IPA is necessary to improve the MAG error measure, whereas it slightly improves the relative difference measure (RDM*). Fuchs *et al* (1998) proposed a weighted IPA approach that used a parameter c to improve accuracy when there are multiple layers in the skull. They have concluded that the parameter mostly depends on the skull conductivity for spherical models. Frijns *et al* (2000) used high-order elements with recursive integration and compared the accuracy of various algorithms on four-layer spherical meshes of different sizes. It was agreed that the use of the IPA is not necessary when quadratic elements are employed. However, the results reported in that study are for a single tangential dipole placed at 80% eccentricity (11 mm away from the cortex). Our results indicate that, for higher eccentricities, that is, when the dipole gets closer to the brain surface, the IPA improves both MAG and RDM* metrics. This behaviour is observed even if quadratic elements are used and recursive integration is applied.

This study contributes to the numerical accuracy of the potential solutions when a multi-compartment tissue model is used inside the skull. In itemized form (1) a generalized formulation of the IPA for multi-layer models is presented, (2) the transfer matrix formulations derived in our previous study (Akalın-Acar and Gençer 2004) are updated to incorporate the generalized IPA, (3) the effects of the IPA on the solution accuracy are tested using spherical models and (4) the effects of the CSF layer and a tumour tissue are explored in a realistic head model. The next section introduces the BEM, formulations of the IPA and presents formulations for calculating the transfer matrices.

2. Boundary element method

2.1. Introduction

In a piecewise homogeneous volume conductor model of the head, the electric potential ϕ and the magnetic field $\vec{B}$ due to a current dipole source $\vec{p}$ satisfy the following integral equations (Geselowitz 1967):

$$\bar{\sigma}\phi(\vec{r}) = g(\vec{r}) + \frac{1}{4\pi}\sum_{j=1}^{L}\left(\sigma_j^- - \sigma_j^+\right)\int_{S_j}\phi(\vec{r}')\frac{\vec{R}}{R^3}\cdot \mathrm{d}\vec{S}_j(\vec{r}'), \tag{1}$$

$$\vec{B}(\vec{r}) = \vec{B}_0(\vec{r}) + \frac{\mu_0}{4\pi}\sum_{j=1}^{L}\left(\sigma_j^- - \sigma_j^+\right)\int_{S_j}\phi(\vec{r}')\frac{\vec{R}}{R^3}\times \mathrm{d}\vec{S}_j(\vec{r}'). \tag{2}$$

In this equation, S_j, $j = 1, \ldots, L$ represents the boundary surfaces between different conductivity regions. σ_j^- and σ_j^+ represent the inner and outer conductivities of S_j, respectively. $\bar{\sigma}$ is the mean conductivity at the field point, $\vec{R} = \vec{r} - \vec{r}'$ is the vector between the field point $\vec{r}$ and the source point $\vec{r}'$, and R is the magnitude of $\vec{R}$. The primary sources g and $\vec{B}_0$ are defined as shown below:

$$g(\vec{r}) = \frac{1}{4\pi\sigma_0}\frac{\vec{p}\cdot\vec{R}}{R^3}, \tag{3}$$

$$\vec{B}_0(\vec{r}) = \frac{\mu_0}{4\pi}\frac{\vec{p}\times\vec{R}}{R^3}, \tag{4}$$

where σ_0 represents the unit conductivity and μ_0 is the permeability of the free space. The second terms in (1) and (2) can be solved numerically by discretizing the surfaces into elements and computing the surface integrals over these elements (Barr *et al* 1966, Barnard *et al* 1967a, 1967b, Geselowitz 1967). In most studies, the elements are chosen as plane triangles on which the potential has either constant or linear variation. A review of these studies has been reported by Ferguson and Stroink (1997). In this study, triangular, quadratic and isoparametric BEM elements are used for discretizing the surface (Gençer and Tanzer 1999). Integrating (1) over all elements, a set of equations are obtained. In matrix notation, this can be expressed as

$$\Phi = \mathbf{g} + \mathbf{C}_0\Phi \tag{5}$$

where Φ is an $N \times 1$ vector of node potentials and N is the number of nodes in the BEM mesh. $\mathbf{C}_0$ is an $N \times N$ matrix whose elements are determined by the geometry and electrical conductivity of the head and $\mathbf{g}$ is an $N \times 1$ vector representing the contribution of the primary sources. To eliminate the singularity in the solution of (5), the method of matrix deflation is employed (Lynn and Timlake 1968). If $\mathbf{I}$ denotes the $N \times N$ identity matrix, then

$$\Phi = (\mathbf{I} - \mathbf{C})^{-1}\mathbf{g} \qquad \Phi = \mathbf{A}^{-1}\mathbf{g}. \tag{6}$$

Here, $\mathbf{C}$ represents the deflated version of $\mathbf{C}_0$ and $\mathbf{A}$ represents $(\mathbf{I} - \mathbf{C})$. After calculating Φ, $\vec{B}$ is computed using Φ through (2). The expression for the magnetic field can be written in matrix notation as

$$\mathbf{B} = \mathbf{B}_0 + \mathbf{H}\Phi. \tag{7}$$

$\mathbf{B}$ is an $n \times 1$ vector representing the magnetic fields at the sensor locations and n is the number of magnetic sensors. $\mathbf{B}_0$ denotes the $n \times 1$ vector of magnetic fields at the same sensor locations for an unbounded homogeneous medium. $\mathbf{H}$ is an $n \times N$ coefficient matrix determined by the geometry and electrical conductivity of the head.

2.2. Isolated problem approach

In a three-layer head model, when the skull to brain conductivity ratio (β) is small ($\beta < 0.1$), the solution of (5) yields numerical inaccuracies. The accuracy of the solutions can be improved using the isolated problem approach (Hämäläinen and Sarvas 1989). In the IPA, the region inside the skull is considered as a homogeneous isolated model. The solution to the original set of equations is expressed in terms of the isolated problem solution and a correction term. In this section, (1) the derivation of the integral equations for the correction terms is extended for a multi-layer head model, (2) the discretized form of the extended modified set of equations is presented and (3) the extended version is simplified to reduce the computation time.

Let us assume that the head model has L layers. The Lth layer is the innermost layer and the $(K-1)$th compartment corresponds to the low-conductivity skull. We will define the surfaces S_1 to S_{K-1} as the *outer* surfaces and S_{K+1} to S_L as *inner* surfaces. The potentials on the inner surfaces are higher than the potentials on the outer surfaces, due to the low conductivity of the $(K-1)$th compartment. To reduce the numerical errors on the potentials of the outer surfaces, Hämäläinen and Sarvas (1989) proposed the following decomposition:

$$\phi(\vec{r}) = \phi'(\vec{r}) + \phi''(\vec{r}) \tag{8}$$

where $\phi''(\vec{r})$ is the solution of the integral equation for the conductor G bounded by S_K (including surfaces S_K to S_L) and $\phi'(\vec{r})$ is the correction term. When ϕ is expressed in the

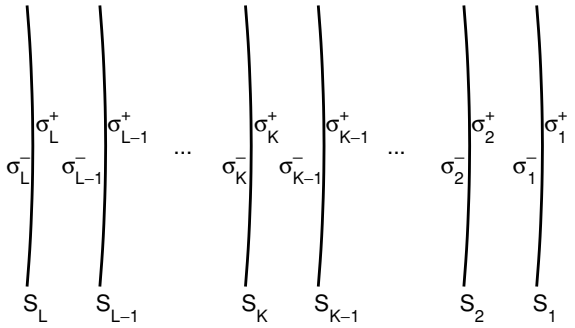

Figure 1. Schematic representation of the model. The model has L layers where the $(K-1)$th compartment has a low conductivity that corresponds to the skull in a head model.

above given form, equation (6) can be written as

$$\Phi' + \Phi'' = \mathbf{A}^{-1}\mathbf{g} \qquad \Phi' = \mathbf{A}^{-1}(\mathbf{g} - \mathbf{A}\Phi'') \qquad \Phi' = \mathbf{A}^{-1}\mathbf{g}'. \tag{9}$$

Decomposing the solution into two parts does not provide any advantage unless the correction term Φ' is solved more accurately as β goes to zero. In such a case, the potentials on the outer surfaces should vanish (this can only be achieved if $\mathbf{g}$ and $\mathbf{A}\Phi''$ cancel each other). However, since the second term is calculated numerically, it is difficult to obtain exact cancellation. The residual error term will be multiplied with $\mathbf{A}^{-1}$ which has a higher condition number due to small β. The IPA is based on the more accurate solution of the right-hand side term $\mathbf{g}'$. The correct behaviour is guaranteed if the right-hand side is calculated as given in Hämäläinen and Sarvas (1989) and Meijs *et al* (1989). Note that, in that representation, each entry on the right-hand side is obtained as a multiple of β.

This section will present the IPA formulation for a general multi-layer model where there are arbitrary numbers of layers inside and outside the low-conductivity layer (figure 1).

For the isolated problem, $\phi''(\vec{r})$ is zero on the surfaces $S_1, \ldots, S_{K-1}$ and the conductivity $\sigma_K^+ = 0$. Therefore, the integral equation for the isolated problem can be expressed as

$$\begin{aligned}\bar{\sigma}''(\vec{r})\phi''(\vec{r}) = g(\vec{r}) &+ \frac{\sigma_K^-}{4\pi}\int_{S_K}\phi''(\vec{r}')\frac{\vec{R}}{R^3}\cdot \mathrm{d}\vec{S}_K(\vec{r}') \\ &+ \frac{1}{4\pi}\sum_{j=K+1}^{L}\left(\sigma_j^- - \sigma_j^+\right)\int_{S_j}\phi''(\vec{r}')\frac{\vec{R}}{R^3}\cdot \mathrm{d}\vec{S}_j(\vec{r}'),\end{aligned} \tag{10}$$

where $\bar{\sigma}''(\vec{r})$ represents the mean conductivity around a point in the isolated-problem space. (Note that the conductivity of the points on S_K is different in the original and the isolated models.) The integral equation for the correction term $\phi'(\vec{r})$ can be obtained by inserting (8) into (1):

$$\bar{\sigma}(\vec{r})(\phi'(\vec{r}) + \phi''(\vec{r})) = g(\vec{r}) + \frac{1}{4\pi}\sum_{j=1}^{L}\left(\sigma_j^- - \sigma_j^+\right)\int_{S_j}(\phi'(\vec{r}') + \phi''(\vec{r}'))\frac{\vec{R}}{R^3}\cdot \mathrm{d}\vec{S}_j(\vec{r}'),$$

$$\begin{aligned}\bar{\sigma}(\vec{r})\phi'(\vec{r}) + \bar{\sigma}(\vec{r})\phi''(\vec{r}) = g(\vec{r}) &+ \frac{1}{4\pi}\sum_{j=1}^{L}\left(\sigma_j^- - \sigma_j^+\right)\int_{S_j}\phi'(\vec{r}')\frac{\vec{R}}{R^3}\cdot \mathrm{d}\vec{S}_j(\vec{r}') \\ &+ \frac{1}{4\pi}\sum_{j=K}^{L}\left(\sigma_j^- - \sigma_j^+\right)\int_{S_j}\phi''(\vec{r}')\frac{\vec{R}}{R^3}\cdot \mathrm{d}\vec{S}_j(\vec{r}').\end{aligned} \tag{11}$$

Combining equations (10) and (11), the following equation can be obtained for the correction terms on the inner and outer surfaces ($i = 1, \ldots, K-1, K+1, \ldots, L$):

$$\left(\sigma_i^- + \sigma_i^+\right)\phi'(\vec{r}) = \frac{1}{2\pi}\sum_{j=1}^{L}\left(\sigma_j^- - \sigma_j^+\right)\int_{S_j}\phi'(\vec{r}')\frac{\vec{R}}{R^3}\cdot \mathrm{d}\vec{S}_j(\vec{r}') - \frac{\sigma_K^+}{2\pi}\int_{S_K}\phi''(\vec{r}')\frac{\vec{R}}{R^3}\cdot \mathrm{d}\vec{S}_j(\vec{r}'). \tag{12}$$

On the Kth surface S_K, $\bar{\sigma}(\vec{r}) = \left(\sigma_K^- + \sigma_K^+\right)/2$ and $\bar{\sigma}''(\vec{r}) = \sigma_K^-/2$. Combining equations (10) and (11) results in the following equation for the corrections on the Kth surface S_K:

$$\begin{aligned}\left(\sigma_K^- + \sigma_K^+\right)\phi'(\vec{r}) = {} & \frac{1}{2\pi}\sum_{j=1}^{L}\left(\sigma_j^- - \sigma_j^+\right)\int_{S_j}\phi'(\vec{r}')\frac{\vec{R}}{R^3}\cdot \mathrm{d}\vec{S}_j(\vec{r}') \\ & - \sigma_K^+\phi''(\vec{r}) - \frac{\sigma_K^+}{2\pi}\int_{S_K}\phi''(\vec{r}')\frac{\vec{R}}{R^3}\cdot \mathrm{d}\vec{S}_K(\vec{r}').\end{aligned} \tag{13}$$

Note that the second term on the right-hand side of (13) is due to the fact that the conductivity of the isolated model on which $\phi''(\vec{r})$ is computed is zero outside the Kth layer. Equations (12) and (13) are equivalent to the IPA expressions derived by Meijs *et al* (1989). By discretizing these integral equations, the following matrix equation can be obtained:

$$\Phi' = \mathbf{g}' + \mathbf{C}\Phi' \tag{14}$$

where Φ' is the $N \times 1$ vector of the correction terms and $\mathbf{g}'$ is an $N \times 1$ vector representing the modified version of the source term. This equation uses the same $\mathbf{C}$ matrix computed for Φ. Using equations (12) and (13), the modified source term $\mathbf{g}'$ can be written in block-matrix form as

$$\mathbf{g}' = \begin{bmatrix} \mathbf{g}'_1 \\ \vdots \\ \mathbf{g}'_{K-1} \\ \mathbf{g}'_K \\ \mathbf{g}'_{K+1} \\ \vdots \\ \mathbf{g}'_L \end{bmatrix} = \begin{bmatrix} \frac{\beta}{\beta-1}\mathbf{C}_{1K}\Phi''_K \\ \vdots \\ \frac{\beta}{\beta-1}\mathbf{C}_{(K-1)K}\Phi''_K \\ \frac{\beta}{\beta-1}\mathbf{C}_{KK}\Phi''_K - \frac{\beta}{\beta+1}\Phi''_K \\ \frac{\beta}{\beta-1}\mathbf{C}_{(K+1)K}\Phi''_K \\ \vdots \\ \frac{\beta}{\beta-1}\mathbf{C}_{LK}\Phi''_K \end{bmatrix}, \tag{15}$$

where $\beta = \sigma_K^+/\sigma_K^-$. In this representation, $\mathbf{g}'_i$ and Φ''_i are the sub-vectors of $\mathbf{g}'$ and Φ'', respectively, where the subscript i stands for the ith surface. Similarly, $\mathbf{C}_{ij}$ represents a sub-matrix of $\mathbf{C}$:

$$\mathbf{C}_{ij} = \frac{1}{2\pi}\frac{\sigma_j^- - \sigma_j^+}{\sigma_i^- + \sigma_i^+}\int_{S_j}\frac{\vec{R}}{R^3}\cdot \mathrm{d}\vec{S}_j(\vec{r}'). \tag{16}$$

An alternative representation for $\mathbf{g}'$ can be obtained by multiplying both sides of (10) with $\beta/\left(\sigma_i^- + \sigma_i^+\right)$ and discretizing the integral equations as follows:

$$\mathbf{g}' = \begin{bmatrix} \mathbf{g}'_1 \\ \vdots \\ \mathbf{g}'_{K-1} \\ \mathbf{g}'_K \\ \mathbf{g}'_{K+1} \\ \vdots \\ \mathbf{g}'_L \end{bmatrix} = \begin{bmatrix} \beta\mathbf{g}_1 + \beta\mathbf{C}_{1(K+1)}\Phi''_{K+1} + \cdots + \beta\mathbf{C}_{1L}\Phi''_L \\ \vdots \\ \beta\mathbf{g}_{K-1} + \beta\mathbf{C}_{(K-1)(K+1)}\Phi''_{K+1} + \cdots + \beta\mathbf{C}_{(K-1)L}\Phi''_L \\ \beta\mathbf{g}_K - \frac{2\beta}{\beta+1}\Phi''_K + \beta\mathbf{C}_{K(K+1)}\Phi''_{K+1} + \cdots + \beta\mathbf{C}_{1L}\Phi''_L \\ \frac{\beta}{\beta-1}\mathbf{C}_{(K+1)K}\Phi''_K \\ \vdots \\ \frac{\beta}{\beta-1}\mathbf{C}_{LK}\Phi''_K \end{bmatrix}, \tag{17}$$

where $\mathbf{g}_i$ can be written as

$$\mathbf{g}_i = \frac{2g(\vec{r})}{\sigma_i^- + \sigma_i^+}. \tag{18}$$

For a three-layer head model, there is only a single layer inside the skull and $K = L = 3$. Thus, the expression given in (17) becomes

$$\mathbf{g}' = \begin{bmatrix} \mathbf{g}'_1 \\ \mathbf{g}'_2 \\ \mathbf{g}'_3 \end{bmatrix} = \begin{bmatrix} \beta\mathbf{g}_1 \\ \beta\mathbf{g}_2 \\ \beta\mathbf{g}_3 - \frac{2\beta}{\beta+1}\Phi''_3 \end{bmatrix} \tag{19}$$

which is the same as the expression derived previously (Hämäläinen and Sarvas 1989).

2.3. Accelerated BEM for EEG

In our previous study (Akalın-Acar and Gençer 2004), we proposed formulations to calculate the EEG and MEG transfer matrices. In that study, we have derived the accelerated BEM formulations when there is a single inner layer. Using that approach, by pre-calculating and storing relevant matrices, we have achieved a significant decrease in the computation time for a given electrode/sensor configuration. In this study, we will generalize these formulations assuming an arbitrary number of inner layers.

If m is the number of electrodes, then the $m \times 1$ vector of electrode potentials can be written as

$$\Phi_e = \mathbf{E}\mathbf{g}' \tag{20}$$

where $\mathbf{E}$ is the $m \times N$ transfer matrix for the electric field. When the IPA is applied, the right-hand side vector $\mathbf{g}$ must be modified using (15). This modification requires Φ''_K that must be calculated for every source configuration using the isolated model:

$$\begin{bmatrix} \Phi''_K \\ \vdots \\ \Phi''_L \end{bmatrix} = (\mathbf{A}_s)^{-1} \begin{bmatrix} \mathbf{g}_K \\ \vdots \\ \mathbf{g}_L \end{bmatrix}. \tag{21}$$

In this equation, $\mathbf{A}_s$ is in the form of $(\mathbf{I} - \mathbf{C_s})$, where $\mathbf{C_s}$ is the deflated coefficient matrix of the isolated inner layers. The vector $[\mathbf{g}_K \cdots \mathbf{g}_L]$ is the corresponding source vector. Note that to compute the node potentials on the outer surface of the isolated model, only the first N_K rows of $(\mathbf{A}_s)^{-1}$ are required. (Here, N_K denotes the number of nodes on that surface.)

To summarize, the accelerated approach for potential field calculations using the IPA starts with the calculation of the transfer matrices $\mathbf{E}$ and $\mathbf{A}_s$. To modify the source vector, $\mathbf{C}_{1K}, \ldots, \mathbf{C}_{LK}$ matrices are also required. Once these matrices are calculated, the potentials due to an arbitrary source configuration can be obtained using the following steps: (1) calculate Φ''_K using (21), (2) calculate $\mathbf{g}'$ using (15) and (3) solve Φ_e using (20).

2.4. Accelerated BEM for MEG

To calculate the magnetic field at the sensor locations from (7), the potential field at all nodes is required. However, using our accelerated BEM formulation (Akalın-Acar and Gençer 2004), it is possible to calculate the magnetic field without calculating the potentials for every source configuration. If n is the number of sensors, then the $n \times 1$ vector of magnetic field measurements can be written as

$$\mathbf{B} = \mathbf{B}_0 + \mathbf{M}\mathbf{g}. \tag{22}$$

Here, the $\mathbf{M}$ matrix is the $n \times N$ *transfer matrix* which relates the source vector $\mathbf{g}$ to the magnetic field measurements.

When the IPA is applied, equation (7) can be rewritten as

$$\begin{aligned}\mathbf{B} &= \mathbf{B}_0 + \mathbf{H}(\Phi' + \Phi'') \\ &= \mathbf{B}_0 + \mathbf{H}\Phi' + \mathbf{H}\Phi'' \\ &= \mathbf{B}_0 + \mathbf{H}\mathbf{A}^{-1}\mathbf{g}' + \mathbf{H}\Phi''.\end{aligned} \tag{23}$$

Since Φ'' is zero for the first $K-1$ layers, we can write $\mathbf{H}\Phi''$ as

$$\mathbf{H}\Phi'' = [\mathbf{H}_1 \dots \mathbf{H}_K \dots \mathbf{H}_L] \begin{bmatrix} 0 \\ \vdots \\ \Phi''_K \\ \vdots \\ \Phi''_L \end{bmatrix} = \mathbf{H}_K \Phi''_K + \dots + \mathbf{H}_L \Phi''_L. \tag{24}$$

Therefore, (23) becomes

$$\mathbf{B} = \mathbf{B}_0 + \mathbf{M}\mathbf{g}' + \mathbf{H}_K \Phi''_K + \dots + \mathbf{H}_L \Phi''_L. \tag{25}$$

In summary, to obtain magnetic field solutions, first the matrices $\mathbf{M}, \mathbf{H}_K, \dots, \mathbf{H}_L, \mathbf{A}_s^{-1}$ and $\mathbf{C}_{1K}, \dots, \mathbf{C}_{LK}$ are computed and stored. After this pre-computation stage, the magnetic field solutions for an arbitrary source distribution can be obtained using (25) with simple matrix–vector multiplications.

3. Results

In this section, first, the accuracy of the numerical solutions obtained using the generalized form of the IPA is tested for a four-layer spherical model. Using a realistic head model (Akalın-Acar and Gençer 2004) and the generalized form of the IPA, the effect of the CSF layer and an inhomogeneity inside the brain on the scalp potentials is explored. The effect of the IPA is investigated using the realistic head model (with an inhomogeneity in the brain). Finally, the computation times for the realistic head model are presented.

3.1. Accuracy

To assess the accuracy of the solutions, a four-layer spherical model is used. The model represents the brain, CSF, skull and the scalp with conductivities 0.33, 1.0, 0.0042 and 0.33 S m $^{-1}$, respectively (Geddes and Baker 1967). The radii of the spheres are chosen as 61, 65, 71 and 75 mm as described in Meijs *et al* (1989). The analytical (V') and numerical (V) solutions are compared using the RDM and RDM* (Meijs *et al* 1989):

$$\%\mathrm{RDM} = \left(\frac{\sum_{i=1}^{m} (V'_i - V_i)^2}{\sum_{i=1}^{m} \left(V'^2_i\right)} \right)^{1/2} \times 100, \tag{26}$$

$$\mathrm{RDM}^* = \left(\sum_{i=1}^{m} \left[\frac{V_i'}{\sqrt{\sum_{i=1}^{m} \left(V_i'^2\right)}} - \frac{V_i}{\sqrt{\sum_{i=1}^{m} \left(V_i^2\right)}} \right]^2 \right)^{1/2}. \tag{27}$$

The BEM mesh used in the simulations has 512 elements and 1026 nodes per layer. To improve the accuracy of the solutions, the recursive integration technique is employed (Frijns *et al* 2000). Accuracy of the numerical solutions is tested with the analytical solutions provided by Kavanagh *et al* (1978). Table 1 shows the percentage RDM and RDM* values for various tangential (x-directed) dipole locations on the z axis (z = 1–6 cm). The numerical solutions are obtained twice (with and without the IPA). It is observed that application of the IPA improves RDM significantly. For deep dipoles, RDM* is relatively small and it is not affected by the application of the IPA. For shallow dipoles, RDM* increases if the IPA is not applied. Table 2 presents the same information for radial dipoles. For the radial shallow dipoles, the increase in the RDM and RDM* is evident.

Table 1. The relative difference measures (%RDMs and RDM*s) for various tangential (x-directed) dipoles located on the z axis (z = 1–6 cm) in a four-layer spherical head model. The results are presented for solutions with and without the IPA.

Distance	With IPA		Without IPA	
(cm)	%RDM	RDM*	%RDM	RDM*
1.0	0.50	0.0006	12.0	0.0060
1.5	0.49	0.0009	12.1	0.0062
2.0	0.49	0.0011	12.2	0.0064
2.5	0.49	0.0015	12.2	0.0066
3.0	0.49	0.0018	12.3	0.0068
3.5	0.48	0.0022	12.4	0.0072
4.0	0.48	0.0026	12.6	0.0087
4.5	0.48	0.0031	12.9	0.0141
5.0	0.49	0.0039	13.8	0.0263
5.5	0.53	0.0046	13.9	0.0384
6.0	1.29	0.0118	16.9	0.1170

Table 2. The relative difference measures (%RDMs and RDM*s) for various radial (z-directed) dipoles located on the z axis (z = 1–6 cm) in a four-layer spherical head model. The results are presented for solutions with and without the IPA.

Distance	With IPA		Without IPA	
(cm)	%RDM	RDM*	%RDM	RDM*
1.0	0.50	0.0009	11.9	0.0059
1.5	0.54	0.0023	11.8	0.0063
2.0	0.69	0.0050	11.7	0.0081
2.5	1.04	0.0093	11.5	0.0122
3.0	1.61	0.0154	11.3	0.0189
3.5	2.36	0.0232	11.2	0.0282
4.0	3.29	0.0325	11.2	0.0399
4.5	4.34	0.0431	11.7	0.0543
5.0	5.49	0.0545	11.9	0.0770
5.5	6.70	0.0640	26.7	0.2370
6.0	9.98	0.0321	227.9	1.8870

3.2. Results with the realistic model

The effects of different tissues on the forward problem are investigated using two simulations. Potentials for a reference BEM model are compared with the potentials for two different head models: the same model (1) without CSF and (2) with an inhomogeneity inside the brain. The results are obtained using the generalized form of the IPA. The effect of the IPA is then investigated when there is an inhomogeneity in the brain. In all simulation studies, a reference head model is used that includes five tissue types. The conductivities of the scalp, skull, CSF, brain and eyes are 0.33, 0.0042, 1, 0.33 and 0.5 S m $^{-1}$, respectively. A 256-electrode Neuroscan cap is used to obtain realistic electrode positions on the scalp surface. The electrode positions are acquired using a Polhemus/Fastrak digitizer and registered to the BEM model.

For realistic models, the error measure MAG is also calculated (Meijs *et al* 1989):

$$\mathrm{MAG} = \left(\frac{\sum_{i=1}^{m} V_i^{\,2}}{\sum_{i=1}^{m} V_i'^{\,2}} \right)^{1/2}. \tag{28}$$

When comparing realistic models, using RDM, RDM* and MAG, V' represents the potential field calculated using the reference head model.

3.2.1. The effect of the CSF layer on the potentials. The effect of the CSF layer on the measurements is investigated by comparing the two models with and without the CSF layer. For the first (reference) model, the solutions are obtained using (15). In the latter model, since there is a single layer in the skull, the IPA is applied as given in (19). The calculations are performed for six dipole locations in both x- and z-directions. Table 3 presents the %RDM, RDM* and MAG. The first column gives the distance of the dipole from the top surface of the brain. It is observed that including the CSF layer in the head model changes the scale of the potentials considerably. However, relatively less change is observed in the field patterns.

3.2.2. The effect of an inhomogeneity in the brain. The effect of an inhomogeneity is investigated when the generalized form of the IPA is applied. The inhomogeneity in the brain is modelled using a spherical region of 1 cm in radius. A cut-away view of the model containing the inhomogeneity is shown in figure 2. The forward problem calculations are performed for a single dipole located at 0.5 cm near the inhomogeneity with parallel and perpendicular orientations with respect to the inhomogeneity surface (figure 3). The comparisons are repeated for varying inhomogeneity conductivities. In table 4, the %RDMs, RDM*s and MAG values are calculated between the forward problem solutions of the two head models with and without the inhomogeneity. It is observed that when the dipole is

Table 3. The %RDMs, RDM*s and MAG values for x- and z-directed dipoles located on the z axis. The potentials of the reference head model are compared with the potentials when there is no CSF layer in the head model.

Distance	x-directed			z-directed		
(cm)	%RDM	RDM*	MAG	%RDM	RDM*	MAG
5.6	32.5	0.13	0.69	446.2	0.18	5.44
4.6	33.4	0.13	0.68	440.2	0.13	5.39
3.6	518.5	0.12	6.18	439.5	0.08	5.39
2.6	507.7	0.12	6.07	445.2	0.04	5.45
1.6	493.4	0.11	5.93	461.9	0.03	5.62
0.6	475.5	0.10	5.75	523.4	0.07	6.23

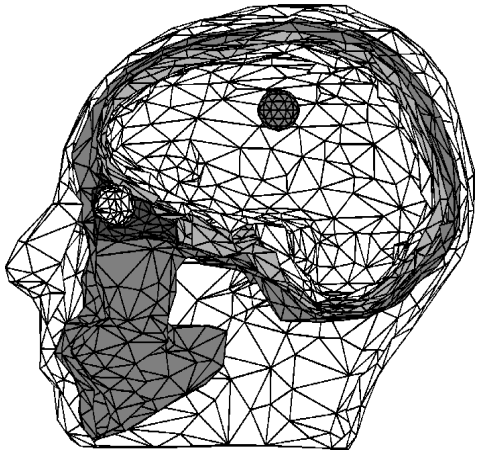

Figure 2. The cut-away view of the head mesh including the inhomogeneity.

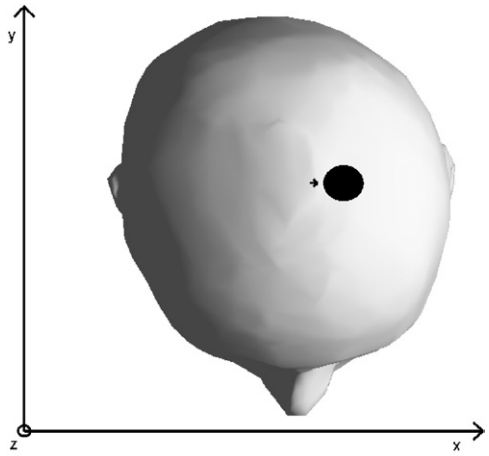

Figure 3. The top view of the head model to show the location of the inhomogeneity and the dipole.

Table 4. Effect of the inhomogeneity on the potential solutions. The potentials using the two head models are compared. %RDMs, RDM*s and MAG values for a dipole located 0.5 cm near the inhomogeneity are presented. The dipole is oriented parallel and perpendicular to the inhomogeneity.

Conductivity	Parallel			Perpendicular		
(S m^{-1})	%RDM	RDM*	MAG	%RDM	RDM*	MAG
0.033	12.24	0.0062	1.12	49.70	0.51	0.87
0.066	10.31	0.0055	1.10	47.82	0.49	0.91
0.165	5.47	0.0037	1.05	44.28	0.44	0.99
0.660	7.83	0.0049	0.92	45.48	0.35	1.24
1.650	17.28	0.0126	0.83	54.97	0.29	1.42
3.300	22.52	0.0181	0.78	61.84	0.27	1.52

Table 5. Effect of the IPA on the potential solutions when inhomogeneity is included. %RDM, RDM*s and MAGs for a dipole located 0.5 cm near the inhomogeneity are presented. The dipole is oriented parallel and perpendicular to the inhomogeneity.

Conductivity ($S\ m^{-1}$)	Parallel			Perpendicular		
	%RDM	RDM*	MAG	%RDM	RDM*	MAG
0.033	552.92	0.12	6.52	545.54	0.29	6.61
0.066	553.00	0.12	6.52	550.68	0.28	6.46
0.165	553.26	0.12	6.52	561.41	0.25	6.58
0.660	554.38	0.12	6.54	580.17	0.20	6.78
1.650	555.58	0.12	6.55	588.29	0.18	6.86
3.300	556.40	0.11	5.56	592.11	0.17	6.90

oriented towards the inhomogeneity, the change in the potential is significant as reflected by the RDM and RDM*. The RDM and RDM* values go through minimum values when the conductivity of the inhomogeneity is assigned as 0.165 S m^{-1} and 0.66 S m^{-1}. These values are the closest values to the brain conductivity among the other conductivity values. As the conductivity of the inhomogeneity differs from the conductivity of the brain, the error measures increase.

3.2.3. The effect of the IPA on the potentials when there is an inhomogeneity. The effect of the IPA is investigated when there is an inhomogeneity in the brain. In table 5, the %RDMs, RDM*s and MAG values are computed between solutions computed with and without the IPA (using the second head model). It is observed that in addition to a considerable change in the scale of the solutions (MAG), the RDM* implies topological differences especially for perpendicular dipoles. (Considering a maximum value of 2 for the RDM*, an RDM* value of 0.29 corresponds to a 15% change in the field pattern.)

For illustrative purposes, the field patterns (the contour plots of the scalp potentials) are also presented for three cases: (1) the reference head model, (2) a model with an inhomogeneity of conductivity 0.033 S m^{-1} and (3) a model with an inhomogeneity of 3.3 m^{-1}. For all three cases, two figures are given (figure 4). The potentials on the left-hand side are computed with the generalized form of the IPA. On the right-hand side, the IPA is not used. It is observed that when the conductivity of the inhomogeneity is low, the overall potential values are reduced. When the inhomogeneity is relatively more conductive, the potential values are increased. An inhomogeneity in the brain causes a shift in the potential pattern towards the inhomogeneity. The inhomogeneity acts like a secondary source and affects the potential pattern accordingly. This behaviour was also discussed previously (Gençer and Acar 2004, Benar and Gotman 2002). When the IPA is not applied, in general, the location of the extrema changes and there are additional unexpected contours (on the lower left side) that show numerical inaccuracies. It is concluded that when the IPA is not applied, the effect of inner layers on the surface potentials is suppressed.

3.3. Computation times

In this section, the computation times for different stages of the forward problem are presented. The computation times are recorded for a specific head model (Akalın-Acar and Gençer 2004) and electrode/sensor configuration (256 electrodes/sensors). The head model includes five different tissue types: the eyes, scalp, skull, CSF and the brain. The corresponding BEM

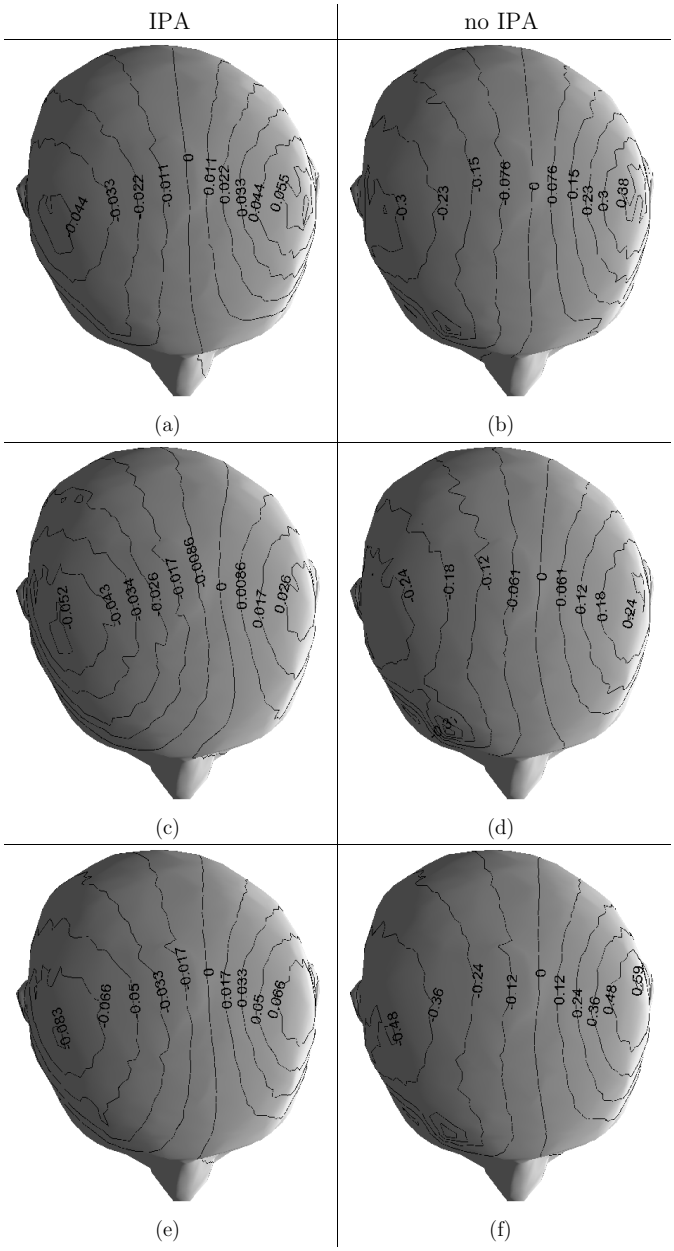

Figure 4. Contour plots on a realistic head mesh with and without IPA for various inhomogeneity conductivities: (a) and (b) no inhomogeneity, (c) and (d) inhomogeneity with low conductivity = 0.033 S m^{-1}, (e) and (f) inhomogeneity with high conductivity = 3.3 S m^{-1}.

mesh has 9906 nodes and 4984 quadratic elements. The solutions are obtained using a nonoptimized iterative solver (biconjugate gradient method). For computations, a 2.4 GHz Pentium IV personal computer (PC) with 1 GB memory is used. The BEM implementation is written using C++ programming language. To calculate the modified source vector in the IPA, equation (15) is used. The sub-matrix corresponding to the *K*th layer of the BEM mesh

Table 6. Computational complexity for a realistic mesh with 9906 nodes, A_s matrix has 3828 nodes.

Matrix filling (**A** matrix)	12 min
Single solution ($\mathbf{A}\Phi = \mathbf{g}$)	3 min
Calculation of **E** (256 electrodes)	3.2 h
Matrix filling ($\mathbf{A}_s$ matrix)	2 min
Calculation of $\mathbf{A}_s^{-1}$ matrix	50 s
Matrix filling (**H** matrix)	28 s
Calculation of **M** (256 sensors)	3.2 h
Calculation of the modified right-hand side (RHS)	3 s
Calculation of the electrode potentials using **E**	3.7 s
Calculation of the sensor fields using **M**	4 s

of the **C** matrix is 1910×9906. Table 6 shows the computation times of various stages. Note that the computation times presented in Akalın-Acar and Gençer (2004) were obtained using a head model with a single layer inside the skull.

4. Conclusions and discussion

To increase the accuracy of the forward problem solutions of EMSI with the boundary element head models, the IPA must be applied. In general, a single layer is assumed in the skull. For realistic head models with arbitrary number of layers in the skull, a generalized version of the IPA is required. In this study, a generalized formulation for the IPA was described. The related integral equations and the discretized version of the modified source terms were presented. In our previous study, we proposed the accelerated BEM approach (Akalın-Acar and Gençer 2004) which improves the solution speed of the EEG and MEG forward problem solutions. The accelerated BEM formulations were updated in this paper to account for the generalized IPA formulations. The accuracy obtained by the new formulation was tested with spherical four-layer models. After validating the IPA for spherical models, the effect of the CSF layer and a tumour tissue was investigated using the generalized form of the IPA in a realistic head model. The effect of the IPA was also investigated for an inhomogeneity in the brain.

Two formulations were derived for the generalized version of the IPA. The matrix equation given in (15) is suitable for a general multi-layer implementation where there are arbitrary numbers of layers in the skull. The integral equations for this case have also been described in Meijs *et al* (1989). However, the alternative form (17) is more efficient when there is a single layer inside the skull layer since no sub-matrices ($\mathbf{C}_{ij}$) need to be stored and used. The matrix equations of the alternative formulation are reduced to the equations given by Hämäläinen and Sarvas (1989) for a three-layer head model.

For a four-layer spherical model, it was observed that the application of the IPA improves the RDM for both deep and shallow dipoles. The improvement in RDM*, however, was apparent for only shallow dipoles. For a radial dipole that is 1 mm close to the brain surface, the RDM* dropped from 1.88 to 0.03. The corresponding %RDM decreased from 227.9% to 9.9%.

Using the realistic head model, we have investigated the effect of three factors on the forward problem solutions: (1) the effect of the CSF layer, (2) the effect of an inhomogeneity with varying conductivities in the brain, (3) the effect of the IPA using a realistic model including an inhomogeneity in the brain. The effect of the CSF layer and the inhomogeneity are investigated by comparing the potentials for a reference BEM model with the potentials for

two different head models: the same model (1) without CSF and (2) with an inhomogeneity inside the brain. It was observed that including the CSF layer changed the scale of the potentials considerably; the field pattern, on the other hand, did not change noticeably. However, the inclusion of an inhomogeneity with 0.033 S m^{-1} changed the scale of the potentials by 50% and the pattern by 25% for a dipole oriented towards the inhomogeneity. It was observed that an inhomogeneity shifts the pattern of the potentials and affects the magnitude of the measurements, in effect acting like a secondary source. Then, the effect of the IPA was investigated when there is an inhomogeneity in the brain. It was observed that in addition to a considerable change in the scale of the potentials, the RDM* also changed by 15%. The application of the IPA also made an observable change in the field profiles. A shift in the location of the extrema was observed. The effect of the IPA on the accuracy of the forward problem was estimated to be more pronounced for realistic head models compared with the spherically symmetric models.

It may be argued whether a low-conductivity inhomogeneity inserted in the isolated region would cause a numerical inaccuracy in the solutions. For a multi-layer inhomogeneity in the brain, the low-conductivity outer layer would decrease the potentials in the inner layers of the inhomogeneity, and an inaccuracy in solutions may be expected. To reduce the inaccuracy, the isolated problem should then be defined for a geometry bounded from two surfaces: the inner surface of the skull layer and the outer surface of the inhomogeneity. In this study, we have not investigated the inaccuracy for such a multi-layer inhomogeneity. However, the accuracy for a single-layer inhomogeneity was tested. For that purpose, a four-layer spherical BEM model representing scalp, skull, brain and a low-conductivity single-layer inhomogeneity (0.033 S m^{-1}) was developed. Since the analytical expression allows source locations only in the innermost shell, we have generated a FEM model (Gençer and Acar 2004, Gençer *et al* 2003) and compared the solutions at the outer surface obtained using the two numerical methods. The RDM was found to be less than 1% for various dipole locations and orientations. Thus, we have concluded that a low-conductivity single-layer inhomogeneity does not cause any numerical inaccuracy in the BEM solutions.

Acknowledgments

This work is supported by the Middle East Technical University Research Fund Projects AFP-2001-03-01-02 and BAP-2003-07-02-00-12. We acknowledge the stimulating questions of an anonymous reviewer of our previous article on the BEM. We would like to thank Dr Can Erkin Acar for reading the manuscript.

References

Akalın-Acar Z and Gençer N G 2004 An advanced boundary element method (BEM) implementation for the forward problem of electromagnetic source imaging *Phys. Med. Biol.* **49** 5011–28

Babiloni F, Carducci F, Cincotti F, Del Gratta C, Pizzella V, Romani G L, Rossini P M, Tecchio F and Babiloni C 2001 Linear inverse source estimate of combined EEG and MEG data related to voluntary movements *Hum. Brain Mapp.* **14** 197–209

Baillet S, Mosher J C and Leahy R M 2001 Electromagnetic brain mapping *IEEE Signal Process. Mag.* **18** 14–30

Barnard A C, Duck I M and Lynn M S 1967a The application of electromagnetic theory to electrocardiology: I. Derivation of the integral equations *Biophys. J.* **7** 443–62

Barnard A C, Duck I M, Lynn M S and Timlake W P 1967b The application of electromagnetic theory to electrocardiology: II. Numerical solution of the integral equations *Biophys. J.* **7** 463–91

Barr R C, Pilkington T C, Boineau J P and Spach M S 1966 Determining surface potentials from current dipoles, with application to electrocardiography *IEEE Trans. Biomed. Eng.* **13** 88–92

Benar C G and Gotman J 2002 Modeling of post-surgical brain and skull defects in the EEG inverse problem with the boundary element method *Clin. Neurophysiol.* **113** 48–56

Budiman J and Buchanan D S 1993 An alternative to the biomagnetic forward problem in a realistically shaped head model, the weighted vertices *IEEE Trans. Biomed. Eng.* **40** 1048–53

Crouzeix A, Yvert B, Bertrand O and Pernier J 1999 An evaluation of dipole reconstruction accuracy with spherical and realistic head models in MEG *Clin. Neurophysiol.* **110** 2176–88

Cuffin B N 1996 EEG localization accuracy improvements using realistically shaped head models *IEEE Trans. Biomed. Eng.* **43** 299–303

Ferguson A S and Stroink G 1997 Factors affecting the accuracy of the boundary element method in the forward problem: I. calculating surface potentials *IEEE Trans. Biomed. Eng.* **44** 1139–55

Frijns J H M, de Snoo S L and Schoonhoven R 2000 Improving the accuracy of the boundary element method by the use of second-order interpolation functions *IEEE Trans. Biomed. Eng.* **47** 1336–46

Fuchs M, Drenckhahn R, Wischmann H A and Wagner M 1998 An improved boundary element method for realistic volume-conductor modeling *IEEE Trans. Biomed. Eng.* **45** 980–97

Geddes L A and Baker L E 1967 The specific resistance of biological material—a compendium of data for the biomedical engineer and physiologist *Med. Biol. Eng.* **5** 271–93

Gençer N G and Acar C E 2004 Sensitivity of EEG and MEG measurements to tissue conductivity *Phys. Med. Biol.* **49** 701–17

Gençer N G, Acar C E and Tanzer I O 2003 Forward problem solution of magnetic source imaging *Magnetic Source Imaging of the Human Brain* ed L Z Lu and L Kaufman (Hillsdale, NJ: Lawrence Erlbaum Associates)

Gençer N G and Tanzer I O 1999 Forward problem solution of electromagnetic source imaging using a new BEM formulation with high-order elements *Phys. Med. Biol.* **44** 2275–87

Geselowitz D B 1967 On bioelectric potentials in an inhomogeneous volume conductor *Biophys. J.* **7** 1–11

Hämäläinen M S and Sarvas J 1989 Realistic conductivity geometry model of the human head for interpretation of neuromagnetic data *IEEE Trans. Biomed. Eng.* **36** 165–71

He B 1998 High-resolution source imaging of brain electrical activity *IEEE Eng. Med. Biol. Mag.* **17** 123–9

Kavanagh R N, Darcey T M, Lehmann D and Fender D H 1978 Evaluation of methods for three-dimensional localization of electrical sources in the human brain *IEEE Trans. Biomed. Eng.* **25** 421–9

Lynn M S and Timlake W P 1968 The use of multiple deflations in the numerical solution of singular systems of equations, with applications to potential theory *SIAM J. Num. Anal.* **5** 303–22

Meijs J W H, Weier O W, Peters M J and Van Oosterom A 1989 On the numerical accuracy of the boundary element method *IEEE Trans. Biomed. Eng.* **36** 1038–49

Michel C M, Thut G, Morand S, Khateb A, Pegna A J, de Peralta R G, Gonzales S, Seeck M and Landis T 2001 Electric source imaging of human brain functions *Brain Res. Rev.* **36** 108–18

Ramon C, Schimpf P, Haueisen J, Holmes M and Ishimaru A 2004 Role of soft bone, CSF and gray matter in EEG simulations *Brain Topogr.* **16** 245–8

Roth B J, Balish M, Gorbach A and Sato S 1993 How well does a three-sphere model predict positions of dipoles in a realistically shaped head? *Electroencephalogr. Clin. Neurophysiol.* **87** 175–84

van Burik M J and Peters M J 2000 Estimation of the electric conductivity from scalp measurements: feasibility and application to source localization *Clin. Neurophysiol.* **111** 1514–21